Real-time retinal tracking for laser treatment planning and administration

Nahed H. Solouma, Abou-Bakr M. Youssef, Yehia A. Badr, and Yasser M. Kadah[1]

Biomedical Engineering Department and Laser Institute, Cairo University, Giza, Egypt

ABSTRACT

We propose a computerized system to accurately point laser to the diseased areas within the retina based on predetermined treatment planning. The proposed system consists of a fundus camera using red-free illumination mode interfaced to a computer that allows real-time capturing of video input. The first image acquired is used as the reference image for treatment planning. A new segmentation technique was developed to accurately discern the image features using deformable models. A grid of seed contours over the whole image is initiated and allowed to deform by splitting and/or merging according to preset criteria until the whole vessel tree is extracted. This procedure extracts the whole area of small vessels but only the boundaries of the large vessels. Correlating the image with a one-dimensional Gaussian filter in two perpendicular directions is used to extract the core areas of such vessels. Faster segmentation can be obtained for subsequent images by automatic registration to compensate for eye movement and saccades. Comparing the two sets of landmark points using a least-squares error provide an optimal transformation between the two point sets. This allows for real-time location determination and tracking of treatment positions.

Keywords: retinal tracking, contour detection, feature extraction, image registration

1. INTRODUCTION

Laser technology has evolved quickly since the first practical system was built in 1960. From then on, laser applications expanded to include numerous industrial, military and medical uses. When laser interacts with biological tissues, it leads to a variety of changes that may include tissue ablation, photocoagulation and/or photodisruption. These changes could be utilized in the treatment of many disorders in almost all branches of medicine, especially in ophthalmology. Because laser can be applied to the posterior as well as the anterior parts of the eye, the range of treatment applications of ophthalmological disorders by lasers has become rather wide. This includes the use of the laser tissue photocoagulation in the treatment of retinal detachment and for the treatment of diabetic retinopathy.

Diabetic retinopathy resulting from long term diabetes mellitus is one of the common diseases that lead to choroidal neovascularization (CNV). CNV is considered among the most important blinding conditions today. It decreases the amount of blood supplying the retina especially within the central area of acute vision [1]. A considerable amount of research has been devoted to overcome this condition. Among the currently available solutions, lasers can be used in the treatment of such disorder by aiming an appropriate amount of laser energy to the affected areas of the retina in order to photocoagulate these areas. To attain satisfactory results, the physician must identify the full extent of CNV and cauterize it completely in order to save the central vision [1-2]. Several thousands of laser shots are required and care must be taken to avoid radiating the macula (the area of acute vision), optic disk, retinal blood vessels or the region between the macula and the optic disk containing the nerve fibers to the area of acute vision. For a single eye, this procedure requires up to several hours that are usually divided over many treatment sessions [22].

Although the treatment of this condition by laser photocoagulation was shown to be superior to the other available methods, it suffers from a number of serious problems. The current success rate of this procedure is below 50% for eradication of CNV following one treatment session with a recurrence and/or persistence rate of about 50% [3-4]. The latter condition requires repeating the treatment. Each treatment repetition in turn has a 50% failure rate. Moreover, several

[1] E-mail: ymk@internetegypt.com

studies indicate that incomplete treatment was associated with poorer prognosis than no treatment [5]. Consequently, the need to develop an automated laser system to treat the whole retina in one session has become a necessity.

In this paper, we propose a new computerized treatment planning system for laser treatment of CNV. The new system has the potential to improve the accuracy of the procedure thus lowering its failure rate while maintaining the same treatment time. A major part of this system is the tracking the retina. This is achieved using a computer-controlled system that captures retinal images from a fundus camera. Novel image processing routines are applied to the retinal images to determine the positions for laser shots on the retina. A fast registration procedure is used to update these positions in case of eye movement. Theses positions can be fed to a beam steering apparatus that precisely directs the laser beam accordingly.

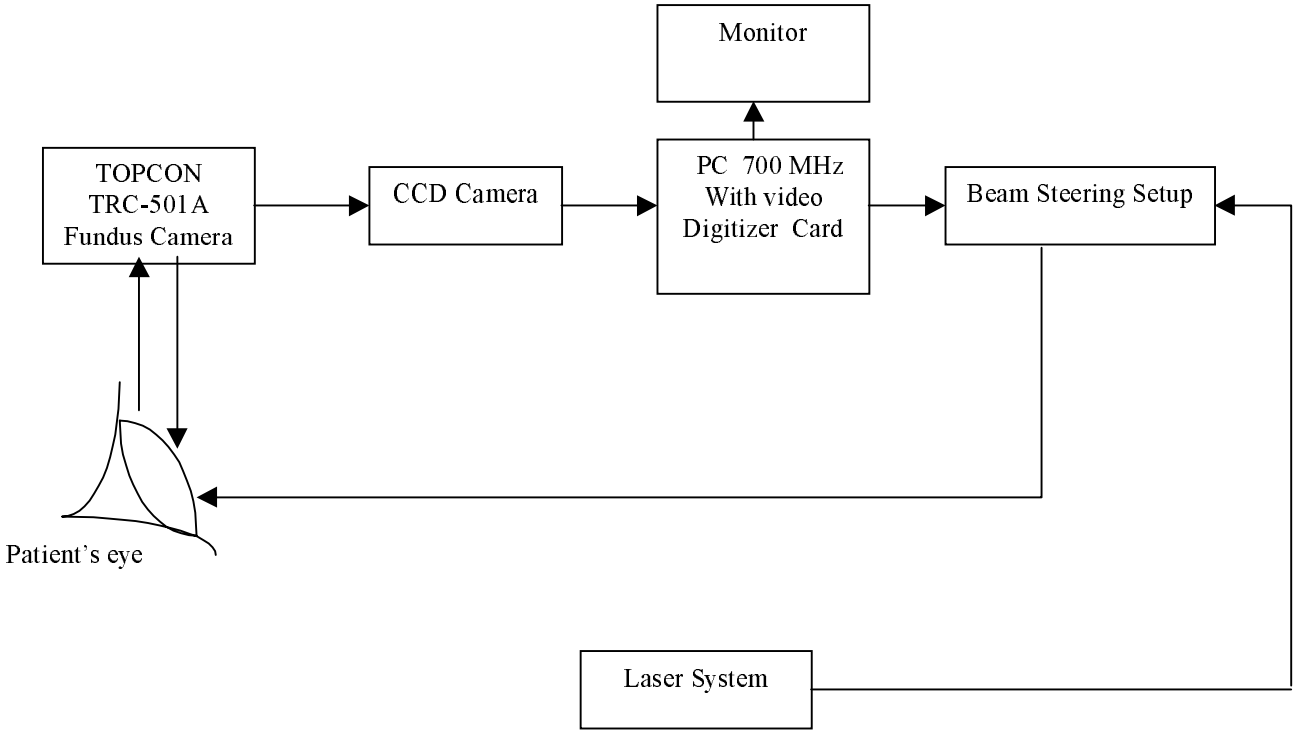

Figure 1. A block diagram for retinal tracking system.

2. BACKGROUND OF RETINAL IMAGE SEGMENTATION

For the computer system to determine the validity of a laser shot position, it must be able to identify the locations for sensitive parts of the retina in the acquired images. This is achieved using image segmentation. In particular, we need to segment the blood vessel tree, optic disc, macula and fovea to ensure that these areas will not be harmed during laser treatment. In the retinal images acquired from fundus camera, the problem of inaccurate segmentation results mainly as a result of non-uniform illumination of the background. Moreover, the variable distance of different retinal areas from the camera causes further degradation because of the expected loss of focus in some areas. These effects cause gray level variations within the same image and gray level differences between different images. This results in significant complications in detecting the blood vessel tree accurately [17].

Several studies have been conducted in the area of blood vessel extraction from retinal images as well as from other medical imaging modalities [7]. Generally speaking, these studies can be classified into two main categories: detection of blood vessel boundaries and extraction of the core of the blood vessel tree by tracing vessel centers.

The first category relies on detecting vessel edges by several techniques. Among those techniques are the use of difference operators and simple thresholding, edge detection based on statistical parameters calculated from the image [9], or edge detection by morphological methods [10,11]. More recent studies perform contour detection using deformable models or *snakes* [12-14]. The detection by difference operators and simple thresholding has been shown to be unreliable due to the existence of small vessels that are not well defined or having poor edges. Also, the detection using image statistics does not perform well when illumination is non-uniform causing variations in the intensity of some blood vessels compared to the image background. On the other hand, morphological methods often lead to a problem of over segmentaion. Contour detection by deformable models has been shown to provide more accurate results. Nevertheless, it requires much longer time in addition to the need for user interaction. This limits to a large degree the practicality of the technique making it unsuitable for real-time applications.

In the second category, the goal is to extract the core of blood vessels. Matching by two-dimensional Gaussian filters is among the techniques within this category [15]. This algorithm requires a large number of computations when the filter is applied in twelve different directions for best performance. Also, steerable filters are used in the detection of the blood vessel core [16,17]. This type of filters is not applied in many directions. Rather, they are applied in only two basic directions and the result is calculated in other directions from a combination of results from these two directions. This has the advantage of fast computation for a reasonable accuracy.

In order to obtain the best results, we propose an algorithm that extracts the blood vessel tree accurately in two steps. First, the boundaries of vessels are obtained and then the core of the wide vessels is determined. Other image features are segmented allowing us to determine the positions for laser shots. These positions are updated during eye movement by registering the two successive frames to get the new coordinates.

3. DATA ACQUISITION SYSTEM

A block diagram of the data acquisition system is presented in Figure 1. The retinal images used in this work were acquired using a TOPCON TRC-501A fundus camera. This camera has three different operating field of view modes of 50, 30, and 15 degree. All images collected for this work were acquired using the 50 degrees mode and with the red-free illumination mode.

A Sony Charge Coupled Device (CCD) video camera was attached to the eyepiece of the fundus camera to make the images collected using the fundus camera available in standard video format. The video output from the CCD camera was interfaced to a Micron PC (700 MHz processor, 128Mbytes of RAM) through a Matrox Meteor video digitizer card. The retinal images were captured to the memory of the computer system by means of a software package called Image Net. This package can capture either individual frames or real time video sequences. The size of the frame is 640x480 pixels of either colored or gray level images. The images were saved on a hard disk for further processing. The image used in this work were gray level images in either the normal case (darker blood vessels on a bright background) or with the patient injected with the Indocyanine Green that gives images with brighter blood vessels relative to a darker background.

4. THEORY AND ALGORITHMS

4.1. Deformable Models

A deformable model is an iterative process in which we initialze a contour model close to the contour of interest. We try to let this contour deform in such a way that it converges to the true contour when it reaches its steady-state position. This is achieved using an iteration that minimizes an energy functional that takes the form:

$$\varepsilon = \Sigma \left(\varepsilon_{\text{internal}}(v(s)) + \varepsilon_{\text{external}}(v(s))\right), \quad (1)$$

where v(s) is a parametrized contour which is normally represented by a discrete set of points or *snaxels*$\{v_1, \ldots\ldots v_n\}$, $\varepsilon_{\text{internal}}(v(s))$ is the internal energy of the contour due to the elastic deformation and bending of the contour, and $\varepsilon_{\text{external}}(v(s))$ represents the energy due to image forces such as lines, edges, termination of line segments and corners [14]. The steady-state position of the deformable contour is the one it takes when its energy is at minimum. The contour model is deformed using one of many algorithms for searching the neighboring points of each snaxel to extract the point of the minimum energy, which will then become the new snaxel [12-14].

In applying deformable models to retinal images to detect the bounderies of the blood vessel tree, the initial contour has to grow and converge to the edges of the vessel. The contour growth could be achieved by interpolating the points on the contour. Different authors used different types of interpolation. For example, this can be performed by taking the middle point between two points [14], or using space partitioning either through marching cubes or triangulation [12]. The latter gives more satisfactory results but it takes much longer time [12]. Also, in order to obtain useful results, many constraints and user interactions were needed which limit the practicality of the procedure. Here, we tried to minimize the number of required computations and making the process as close to being automatic as possible at the highest attainable accuracy. So, we studied the effect of the internal energies and compared it with the effect of the external energy (edge energy in this case) to make sure that the effect of the external energy will be dominant. The image was convolved by a Sobel operator in both the horizontal and vertical directions. The magnitude of the result was used to represent the external energy of the contour. Instead of selecting a single point having the minimum energy (i.e., maximum edge value) from the neighborhood of each snaxel, we search all the neighboring points of each snaxel and extract all the points having a value above certain threshold as new points on the contour. This not only deforms the contour but also makes it grow. Figure 2 shows an example of applying this algorithm on a red-free image in the normal case. Figure 2.a presents the original image with the initial contour appearing as a small circle near to the edges of a blood vessel. The rest of this figure shows the growth of the contour. Figures 2.b-d show the contour after 1, 50, and 100 iterations respectively. Figure 3 illustrates that if we initialize a contour away from a true edge, it will vanish. This property could be utilized in selective detection of some bondaries and neglecting the others. In Figure 4, we initialize the contour around the edges of a pathologic area to selectively detect the contour within this area.

a. Initial Contour

b. Contour after one iteration

c. Contour after 50 iterations

d. Contour after 100 iterations

Figure 2. Illustration of contour growth

3.a. the initial contour is away from a true

3.b. No detected contour

Figure 3. Illustration of the effect of proper placement of the initial contour

4.a. Initial contour placed nearer to a pathology

4.b. The pathologic area is determined

Figure 4. Selectivity of contour detection

4.2. Detection of blood vessel boundaries

Instead of manual initialization of contours, the whole image was covered automatically with an initial set of small contours called *seed* contours (see Figure 5) [12]. During the contour iteration convergence and growth, the seed contours that lie within the areas of poor edges shrink until vanishing. The others will merge and/or split until recovering a continuous description of all edges that pass above a certain threshold. This threshold changes with every iteration to allow for faster and more accurate convergence. This process is repeated until no changes occur during a given iteration. This process leads to the complete detection of all small vessels in addition to the boundaries of the larger ones.

4.3. Core Finding Algorithm

The intensity values across a blood vessel are usually assumed to have a Gaussian distribution. On the other hand, the small segments usually have repeated intensity values [15]. So, correlating the image with two-dimensional filters of suitable size (e.g., 16x15) constructed from two one-dimensional Gaussian filters in two perpendicular directions can be utilized to match the segments across the blood vessel [15]. This process provides reasonable results but it requires a large number of computations to detect all vessels. In particular, the filter has to be applied in 12 different directions to be able to detect vessels in all possible directions. In this work, since we detect the small vessels and the boundaries of the wider vessels at an earlier step, we only need to obtain the core of the wide vessels. Therefore, we only have to correlate the image with two one-dimensional Gaussian filter in the vertical and the horizontal directions only. This reduces the computational complexity of the original technique to a great extent and makes it practical for clinical applications. Figures 5 and 6 show the seed contours and the result of applying this technique.

4.4. Segmenting the optic disc

The optic disc is a well-delineated object with properly defined size and edges [24]. The nerve fibers and blood vessels enter the retina through the optic disc. In the gray level retinal images, it always appears as an nearly circular structure that is brighter than the background of the retina. We manually selected the central point of the optic disc and taking a window around that point. The points inside this window were taken to be the expected centers of the optic disc. We determined a larger window around the initial point and the edge points inside this window were calculated and assumed as the expected points on the circumference of the optic disc. We applied the Hough transform [24], which is well known as a robust method to extract circular objects, to detect the center and the radius of optic disc. A circle was drawn around the optic disc and this circle was filled to distinguish this structure.

4.5. Segmenting the macula

The macula is the area of acute vision within the retina. It appears as the most homogeneous area near the optic disc. To segment the macula, we manually selected a point in the fovea (the center of the macula), then by a region-growing algorithm, the macula was extracted as the connected region around the fovea having intensities near the intensity of the central point. The radius of this region was taken to be double the size of the radius of the optic disc in the y-direction and three times the same radius in the x-direction [24]. Figure 7 shows the result of applying such processes.

4.6. Estimating the locations of laser shots

After extracting all of the sensitive objects above that must be avoided during laser treatment, a binary image was composed containing these objects. This image was dilated by a square structuring element of dimensions 7x7 to maintain a safety margin around these sensitive areas. The locations of shots were determined and spaced in the background. These locations were stored in the database of the patient and get updated with every successive image frame [22].

4.7. Real time movement tracking

Since the segmentation step is a rather time consuming task, it is difficult to rely on it to track fast eye movements particularly during the laser treatment session. Alternatively, we used segmentation for only the first reference retinal image and then the segmentation of any subsequent frame is obtained through a fast registration step. That is, we take advantage of the fact that the eye movements are expected to be slight and perform a simple registration procedure to estimate the motion parameters. Once these parameters are obtained, the segmentation of the first frame only needs to be transformed using these parameters to compute the segmentation for the other frame. Therefore, image registration is an important task that will be performed in real time to compensate for eye movements and saccades. We used the Sequential Similarity Detection Algorithm (SSDA) to obtain similar points [20]. As mentioned above, we extracted the optic disc by determining its center and its radius and this was done in the first frame. Then we used the center of the optic disc as a landmark point. Another landmark was chosen manually at a wide vessel branch. A window was taken around every landmark and then an error function is computed for the following image frame. This error functions is defined as,

$$\varepsilon(i,j,l_n,m_n) = \left| S_M{}^{i,j}(l_n,m_n) - \bar{S}(i,j) - W(l_n,m_n) + \bar{W} \right|, \quad (2)$$

where the dimension of the window $W(l_n,m_n)$ is MxM, $n = 1,2,3,\ldots..M^2$, $\bar{W}$ is the mean gray level value within W, S is the search region in the following frame centered at i,j and S gives the mean gray level value at i,j [20]. The array containing the error function was searched for the point of minimum value corresponding to the center point of the window. This process was repeated for the two windows. Hence, together with the center point of the optic disk, we now have a set of two landmark points within each image frame. The x and y coordinates of the center of gravity of these two points were calculated in the two successive frames to derive the shifts in the x and y directions. The rotation is calculated as the difference between the slopes of the line connecting the two points with respect to the horizontal axis in the two successive frames. The locations of the laser shots that had been estimated from the first frame were updated to their corresponding locations in the successive frame based on this simple transformation.

5. RESULTS AND DISCUSSION

5.1. Results of blood vessel tree segmentation

Figure 5 shows an example of applying the proposed algorithm on an Indocyanine Green image, which appears as bright blood vessels in a dark background. As can be observed, the vessels are accurately extracted even when they are small and without sufficient contrast. This is because the utilized threshold changes locally according to the maximum edge value. Moreover, this algorithm is close to being automatic and involves minimal user interaction. In Figure 6, we present another example of applying the same algorithm on a normal case image (i.e., with no injected dye). As shown in this image, the blood vessels appear as dark objects in a bright background. Because the intensity distribution across the blood vessels is assumed Gaussian, a Gaussian filter was used in matching large vessel cross sections. Instead of using two-dimensional filters in twelve different directions, we used only one-dimensional filter in two perpendicular directions to extract the core of the wide vessels. This reduces the time and computation effort.

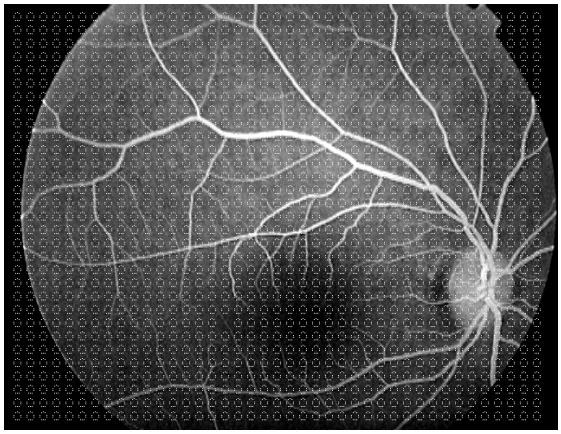

Figure 5.a: Seed contours

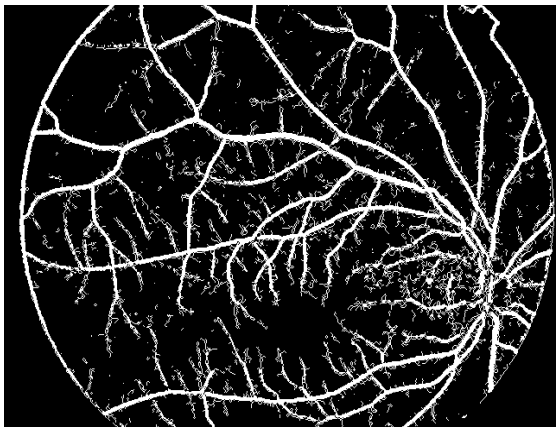

Figure 5.b: Extracted blood vessel

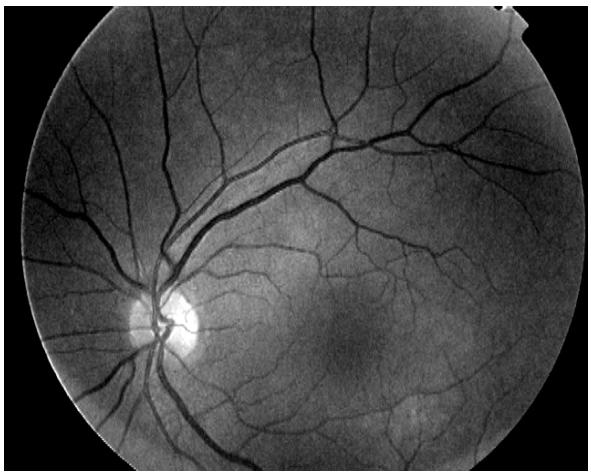

Figure 6.a: Original image

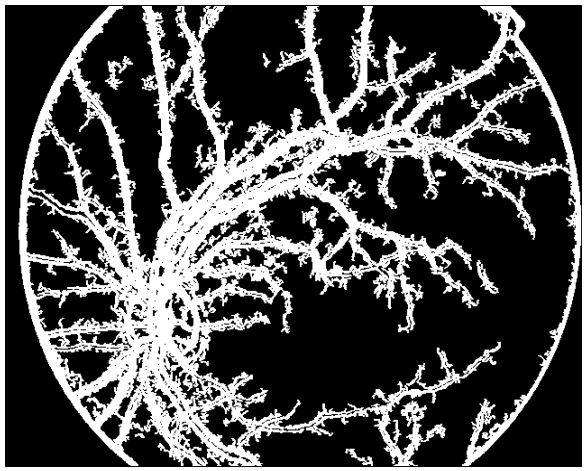

Figure 6.b: Extracted blood vessel tree

5.2. Results of Segmenting the Optic Disc and the Macula

The optic disc is a circular structure in the normal case. However, in some diseased cases, its shape may be deformed. We used the Hough transform to detect the optic disc as a circle-shaped structure and utilized a higher value than the one estimated using this method to ensure that the optic disc lies completely inside the estimated circle. We assumed that it is sufficient to extract the optic disc this way because we dilate the extracted objects for safety. Extraction of non-circular optic disc will be considered as future work.

The macula is the most sensitive object that must be avoided during laser treatment. Consequently, we not only it was demarcated but also its bounds were enlarged to have a double the diameter of the optic disc in the y-direction and three times the same distance in the x-direction. Figure 7 shows the results of extracting the optic disc and demarcating the macula in the above images. The enlargement of the macula is not shown in this figure.

5.3. Results of Tracking the Retina and Location Updating

The tracking algorithm considered here is based on image registration. Here, we consider the retina to move as a rigid body (this is usually close to reality except in cases of retinal tears). During image capturing, the patient is asked to fixate his eye with respect to the camera in order to get the same scale in all image frames. So, we are only interested in estimating the shift and angle of rotation between frames. The angle of rotation is always around and does not usually exceed 5 degrees. The resultant angle of rotation and the estimated shift always compensate for each other, so we could rotate the locations of shots around any point in the image plane. We calculate the shift at the center of gravity of the two landmark points and rotated the estimated positions around it. In this method of tracking, we need to select the landmarks manually. But this is only in the first frame and the process proceeds automatically in the following frames because the points estimated within a frame will be used to estimate the corresponding points in the successive frame. A validation algorithm has to be implemented for this algorithm to make sure of the accuracy of the transformation. Figure 8 and 9 show the results of transforming the positions to a following frame.

6. CONCLUSIONS

A new computerized technique for laser treatment planning was proposed. The new technique performs fast segmentation on a reference frame and use fast registration to compute the segmented images of the sequence of images acquired during the treatment. This enables fast tracking of retinal structures and ensures proper administration of the treatment in case of eye movement. Future work is needed to resolve some of the special cases not addressed by this technique such as non-circular optic disk shape.

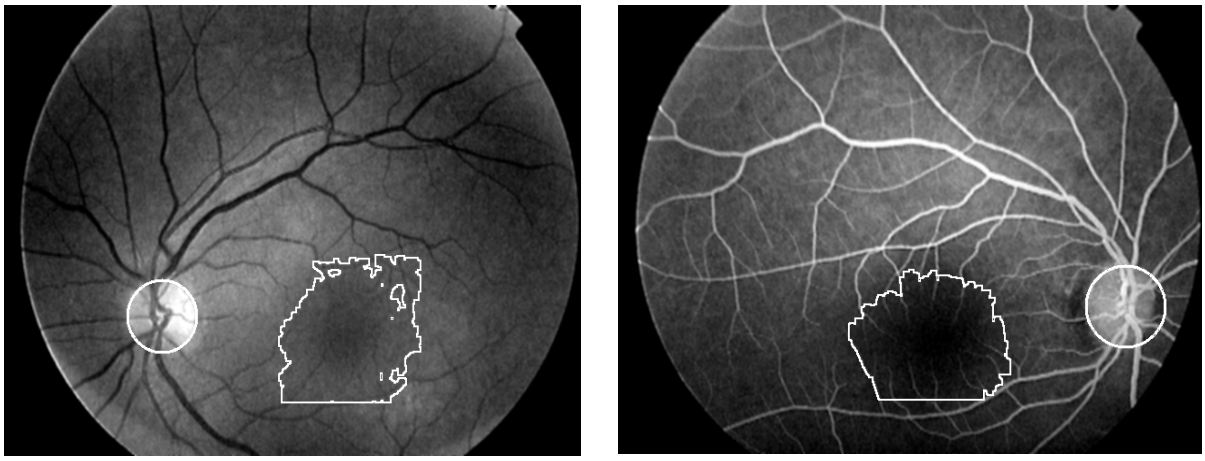

Figure 7. Demarcation of the optic disc and macula

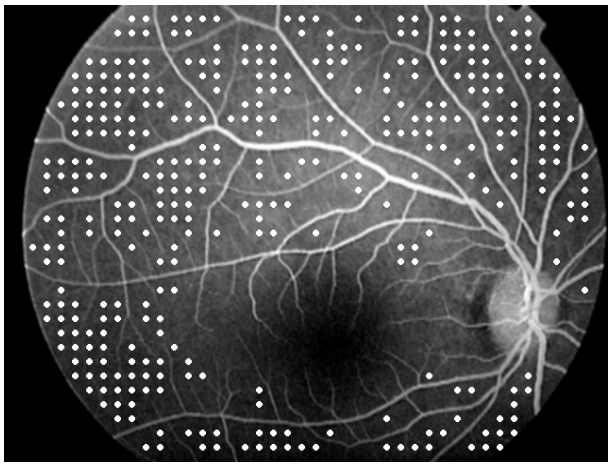

Figure 8.a. Positions of shots in a dye injected image

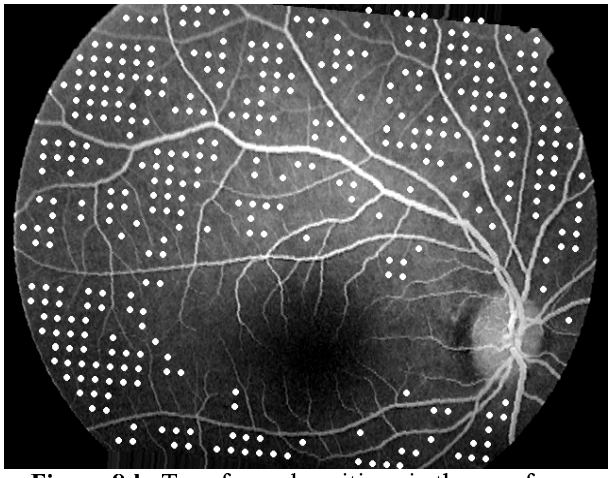

Figure 8.b. Transformed positions in the new frame

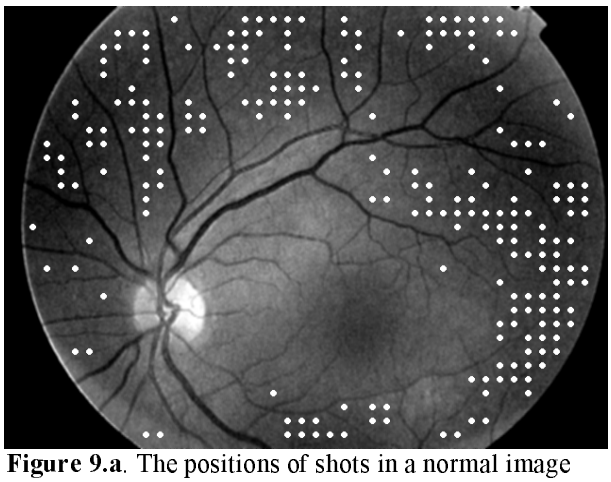

Figure 9.a. The positions of shots in a normal image

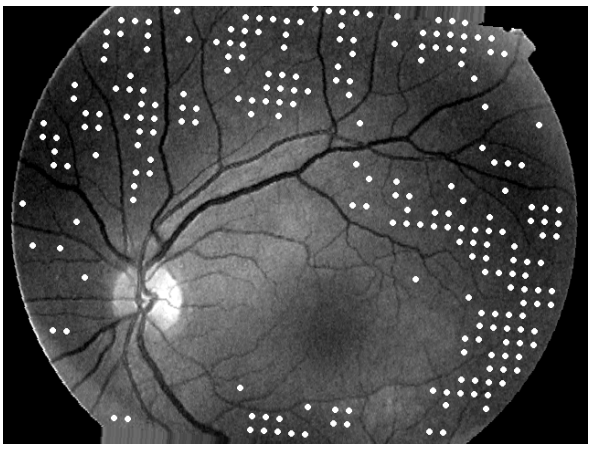

Figure 9.b. The transformed positions in the new frame

Appendix I: Pseudo code for the proposed segmentation technique

```
1.  Generate the seed contour array
2.  Structuring element = 3x3 array of one's
3.  Smooth the image
4.  Get the Gradient Image
5.  Th = max(Gradient image)/threshold
6.  Set NoChanges to false and Final Contour Image array to zeros
7.  WHILE Threshold  > 1 DO
8.    while NoChanges  = FALSE do
9.      temporary Contour Image = Contour Image
10.     Dilate the Contour Image by the Structuring element
11.     Contour Image = Contour Image AND Image Gradient > Th
12.     If  temporary Contour Image = Contour Image Then NoChanges = TRUE
13.   End of while
14.   Gradient Image  =  zeros where Contour Image =  1
15.   Final Contour Image  = Final Contour Image + Contour Image
16.   Threshold = Threshold/2
17.   Th = max(Gradient Image)/Threshold
18. END of WHILE
```

Appendix II: Example of computational requirements of segmentation algorithm

A Pentium III 700 was used to compute the results using the algorithm in Appendix I.

For the image shown in Figure 5:

- The Threshold is set to 7.0.
- With the first Th value: NoChanges is set to TRUE after 52 iterations taking 2.3 seconds.
- With the second Th value: NoChanges is set to TRUE after 30 iterations taking 1.3 seconds
- With the third Th value: no changes is set to TRUE after 2 iterations and it takes 0.1 seconds

Total feature segmentation time is 3.9 seconds for reference image.

For the image shown in Figure 6,

- The threshold is set to 10.0
- With the first Th value: NoChanges is set to TRUE after 98 iterations taking 4.2 seconds
- With the second Th value: NoChanges is set to TRUE after 93 iterations taking 4.0 seconds
- With the third Th value: NoChanges is set to TRUE after 2 iterations taking 0.11 seconds
- With the fourth Th value: NoChanges is set to TRUE after 1 iteration taking 0.09 seconds

Total feature segmentation time is 8.6 seconds.

REFERENCES

1. Macular Degeneration Study Group, "Recurrent choroidal neovascularizaion after argon laser photocoagulation for neovascular maculopathy," *Arch. Ophthalmol.*, **104**, pp. 503-12,1986
2. S.L. Trokel, "Lasers in Ophthalmology," *Optics,Photonics News*, pp. 11-13, Oct. 1992.
3. N.M. Bressler, S.B. Bressler, and E.S. Gragoudas, "Clincal characteristics of choroidal neovascular membranes," *Arch. Ophthalmol.*, **105**, pp. 209-213, 1987.
4. P.N. Monahan, K. A. Gitter, and G. Cohen, "Evaluation of Persistence of Subretinal Neovascular Membranes Using Digitized Angiographic Analysis," *Retina-J. Retinal, Vitreous Diseases*, **13**, no. 3, pp. 196-201, 1993.
5. S. Fine, "Observations Following Laser Treatment for Choroidal Neovascularization," *Arch. Ophthalm.*, **106**, pp. 1524-1525, 1988.
6. T.M. Clark, W. R. Freeman, and M. H. Goldbaum, "Digital Overlay of Flourescein Angiograms and Fundus Images for Treatment of Subretinal Neovascularization," *J. Retinal, Vitreous Diseases*, **2**, no. 12, pp. 118-126, 1992.
7. L.S. Davis, "A Survay of Edge Detection Techniques," *Comp. Graph. Imag. Proc.*, **4**, pp. 248-270, 1975.
8. D.E. Becker, A. Can, J.N. Turner, H.L. Tannenbaum and B. Roysam, "Image Processing Algorithms for Retinal Montage Synthesis, Mapping, and Real-Time Location Determination," *IEEE Trans. Biomed. Eng.*, **45**, no. 1, pp. 105-117,1998.
9. E. Aniram, H. Aydinoglu, and I. C. Goknar, "Decision Based Directional Edge Detector," *Signal Proc.*, **35**, pp. 149-156, 1993.
10. F. Meyer and S. Beucher, "Morphological Segmentation," *J. Visual Comm. Imag. Representation*, **1**, no. 1, pp. 21-46, 1990.
11. R.M. Haralick, S.R. Sternberg and X. Zhuang, "Image Analysis Using Mathematical Morphology," *IEEE Trans. Pattern Anal. Machine Intelligence*, **PAMI-9**, no. 4, pp.532-550, 1987.
12. T. McInerney and D. Terzopoulos, " Deformable Models in Medical Image Analysis: aSurvay," *Med Image Analysis*, **1**, no. 2, pp. 91-108, 1996.
13. T. McInerney and D. Terzopoulos, "Topologically Adaptable Snakes," *Computer Vision (ICCV)*, pp. 840-840, June 1995.
14. J. Schnabel, "Active Contours, Snakes, or Deformable Curves," *Ph.D. Dissertation*, Universite Paris—Sud, 1997.
15. S. Chaudhuri, C. Chatterjee, Norman Katz, Mark Nelson, And Michael Goldbaum, "Detection of Blood Vessels in Retinal Images Using Two-Dimensional Matched Filters," *IEEE Trans. Med. Imaging* **8**, no. 3, pp.263-269, 1989.
16. W.T. Freeman, E.H. Adelson, "The Design and Use of Steerable Filters," *IEEE Transaction on Pattern Analysis and Machine Intelligence*, **13**, no. 9, pp.891-906, 1991.
17. B. Kochner, D. Schuhmann, M. Michaelis, G. Mann, K.-H. Englmeier, "Course Tracking and Contour Extraction of Retinal Vessels from Color Fundus Photographs: Most Efficient Use of Steerable Filters for Model Based Image Analysis," *SPIE Conf. Image Processing*, **3338**, pp. 755-761, 1998.
18. Q. Zheng, and R. Chellappa, "A Computational Vision Approach to Image Registration," *IEEE Trans. Image Processing*, **2**, no. 3, pp. 311-326, 1993.
19. P. Dani and S. Chaudhuri, " Automated Assembling og Images: Image Montage Preparation," *Pattern Recognition*, **28**, no. 3, pp. 431-444, 1995.
20. D.I. Barnea and H.F. Silverman, "A Class of Algorithms for Fast Digital Image Registration," *IEEE Trans. Computers*, **C-21**, no.2, pp.179-186, 1972.
21. B. Peli, R.A. Augliere and G.T. Timberlake, "Feature-Based Registration for Retinal Images," *IEEE Trans. Med. Imaging*, **MI-6**, no. 3, pp.272-278, 1987.
22. S.F. Barrett, M.R. Jerath, H. Grady Rylander III and Ashley J. Welch, "Digital Tracking and Control of Retinal Images," *Optical Engineering*, **33**, no.1, pp.150-159, 1994.
23. M.S. Markow, H. Grady Rylander III, and A. J. Welch, " Real_Time Algorithm fo Retinal Tracking," *IEEE Trans. Biomed. Eng.*, **40**, no. 12, pp. 1269-1281, 1993.
24. A. Pinz, S. Bernogger, P. Datlinger, and A. Kruger, " Mapping the Human Retina," *IEEE Trans. Med. Imaging*, **17**, no. 4, pp. 606-619, 1998.